Available online at www.sciencedirect.com

ScienceDirect

Physics Procedia 56 (2014) 117 – 124

Physics Procedia

8th International Conference on Photonic Technologies LANE 2014

Direct selective laser sintering/melting of high density alumina powder layers at elevated temperatures

J. Deckers[a], S. Meyers[a,*], J.P. Kruth[a], J. Vleugels[b]

[a]KU Leuven, department of mechanical engineering, division PMA, Celestijnenlaan 300, 3001 Heverlee, Belgium
[b]KU Leuven, department of materials engineering, division SIEM, Kasteelpark Arenberg 44 bus 2450, 3001 Heverlee, Belgium

Abstract

Direct selective laser sintering (SLS) or selective laser melting (SLM) are additive manufacturing techniques that can be used to produce three-dimensional ceramic parts directly, without the need for a sacrificial binder. In this paper, a low laser energy density is applied to SLS/SLM high density powder layers of sub-micrometer alumina at elevated temperatures (up to 800°C). In order to achieve this, a furnace was designed and built into a commercial SLS machine. This furnace was able to produce a homogeneously heated cylindrical zone with a height of 60 mm and a diameter of 32 mm. After optimizing the layer deposition and laser scanning parameters, two ceramic parts with a density up to 85% and grain sizes as low as 5 μm were successfully produced.

Peer-review under responsibility of the Bayerisches Laserzentrum GmbH
Keywords: Alumina; Ceramics; Additive manufacturing; Selective laser sintering; Selective laser melting; Electrophoretic deposition; Preheating

1. Introduction

Ceramic material is conventionally processed through a powder metallurgy (PM) process, consisting of (1) powder production, (2) primary shaping, (3) de-binding, (4) furnace sintering and (5) final shaping. This is summarized in figure 1. Primary shaping is traditionally done by slip casting or injection moulding. However, recent developments in additive manufacturing (AM) technologies have made it possible to shape ceramic parts in geometries and forms that cannot be achieved by the traditional techniques. Laser based rapid manufacturing technologies, like selective laser sintering (the laser beam partially melts the powder particles, SLS) or selective laser melting (the laser beam fully melts the powder particles, SLM), are very promising in this area and could perform the primary shaping step in the PM process for small series of complex parts. Two different types of selective laser sintering (SLS) can be distinguished: indirect SLS (iSLS) and direct SLS (dSLS).
In iSLS, ceramic powder is mixed with a polymer binder. The resulting powder can be used as such (dry) or suspended in a liquid to obtain a slurry (wet). The dry powder or slurry is then deposited and laser scanned layer by layer. The laser scanning melts the polymer binder, 'glueing' the ceramic particles together in the process. The sacrificial

* Corresponding author. Tel.: +32 16 37 91 68 .
E-mail address: sebastian.meyers@kuleuven.be

Peer-review under responsibility of the Bayerisches Laserzentrum GmbH
doi:10.1016/j.phpro.2014.08.154

polymer binder is then removed from the green part during the de-binding process. Finally, the resulting ceramic part is sintered in a furnace. Subramanian et al. (1995) performed iSLS on an alumina/polymer powder system and produced alumina parts with densities up to 50 % and strengths of 8 MPa. A decade later, Liu et al. (2007) used ball-milled mixtures of alumina and stearic acid to manufacture ceramic bars with densities up to 88 % and flexural strengths of 255 MPa. Leu et al. (2012) performed iSLS on zirconium diboride powders mixed with stearic acid binder to produce ceramic parts with average densities of 87 % and average flexural strengths of 250 MPa. The iSLS process can be combined with post-processing techniques to further increase densities and improve final mechanical properties. Typical post-processing techniques are isostatic pressing (Liu et al. (2013)) and infiltration (Shahzad et al. (2013)). Recently, slurry-based iSLS processes are being chosen over powder-based variants. Tang et al. (2011) proved that alumina ceramic parts with densities up to 98 % and average flexural strengths of 363.5 MPa can be produced by performing iSLS on a slurry composed of alumina powder coated with polyvinyl-alcohol (PVA). It appears that slurry-based processes (which are colloidal processes since the slurries consist of ceramic particles smaller than 1 μm) can produce highly dense ceramic parts more easily.

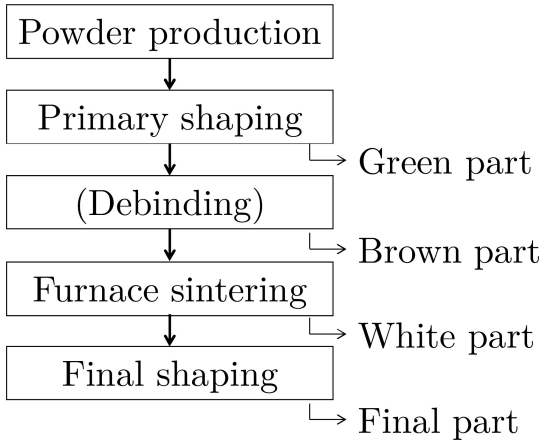

Fig. 1: The PM process.

In direct SLS/SLM, no polymer binder is used. The ceramic particles are deposited and laser scanned layer by layer. The interaction of the laser with the ceramic particles will cause the particles to bind together if the applied laser energy density is sufficiently large. Afterwards no de-binding or furnace sintering is required. Bertrand et al. (1997) investigated the influence of powder characteristics and direct SLS/SLM process parameters on the final properties of zirconia parts. They were able to produce zirconia parts with densities up to 56 %. Wilkes et al. (2013) combined SLM of zirconia-alumina powders with preheating temperatures of up to 1800°C. In this way, ceramic objects with near 100 % density and flexural strengths up to 538 MPa were made. However, the surface quality and dimensional accuracy were poor.

In this paper, high density powder layers are deposited through electrophoretic deposition (EPD) of a ceramic slurry (colloid). High preheating temperatures (800°C) are combined with direct SLS/SLM to rapidly produce three dimensional alumina parts. The EPD layer deposition combined with high preheating temperatures ensured that only a small laser energy density was necessary to fuse the alumina particles together. In this way, large grain sizes and high thermal gradients could be avoided.

Nomenclature

d_{1/e^2}	Laser beam diameter $(1/e^2)$ [μm]
d_{50}	Median particle diameter [μm]
d_e	Distance between electrophoretic deposition electrodes [cm]
l	Layer thickness [μm]
P	Laser power [W]
s	Scan spacing [μm]
T	Preheating temperature [$^\circ C$]
t_d	Deposition time [s]
U	Electrophoretic deposition voltage [V]
v	Scan speed [mm/s]

2. Experimental procedures

2.1. Materials and Slurry Preparation

High purity α-Al_2O_3 powder (SM8 grade, Baikowski, France) with a d_{50} of 0.3 μm was used as the primary structural material. For the EPD process, a slurry with 5 *vol%* of the SM8 α-Al_2O_3 powder, 95 *vol%* of Disinfectol (denatured ethanol with up to 5 *vol%* ether, Chem-Lab, Belgium) and 1.5 *mM* of HNO_3 (Chem-Lab, Belgium) was prepared. The nitric acid was added to provide positive charging of the Al_2O_3 particle surfaces. This resulted in an electrostatic repulsion between the charged particles and improved the stability of the suspension. The slurry was deagglomerated at 70 *rpm* for 12 *hours* using a Al_2O_3 milling balls in a Turbula mixer (Type T2A, WAB, Basel, Switzerland). The slurry could then be deposited in an experimental EPD set-up.

2.2. Layer Deposition

The layer deposition process can be subdivided into two steps. In a first step, a highly dense powder layer was deposited on a cylindrical deposition electrode through the electrophoretic deposition (EPD) process. EPD is a colloidal processing technique since it uses a slurry containing ceramic particles smaller than 1 μm as a starting material. During EPD, non-agglomerated, sub-micrometer powder particles can be densely packed and homogeneously deposited. The EPD process took place in an EPD cell, which contained the slurry with positively charged alumina particles. The deposition electrode was at the top of this EPD cell, while a counter electrode was mounted at the bottom. By negatively charging the deposition electrode and positively charging the counter electrode, the positively charged sub-micrometer alumina particles in the slurry moved to the deposition electrode and formed a densely packed powder layer. For this layer deposition process, an *EPD-voltage (U)* of 150 *V* and a *deposition time (t_d)* of 40 *s* were used. The *distance between the electrodes (d_e)* was kept at 4.3 *cm*. With these parameters, layers with a *thickness (l)* of 50-200 μm could be produced. This is summarized in table 1. The EPD cell assembly is presented on figure 2.
In a second step, the deposited layer was transferred to the (modified) building platform of a DTM Sinterstation 2000 machine. This was accomplished by friction, causing the EPD'-ed powder layer to slide off the deposition electrode and onto the previously deposited and laser scanned powder layers.

Table 1: Electrophoretic deposition parameters.

U	**d_e**	**t_d**	**l**
150 *V*	4.3 *cm*	40 *s*	50-200 μm

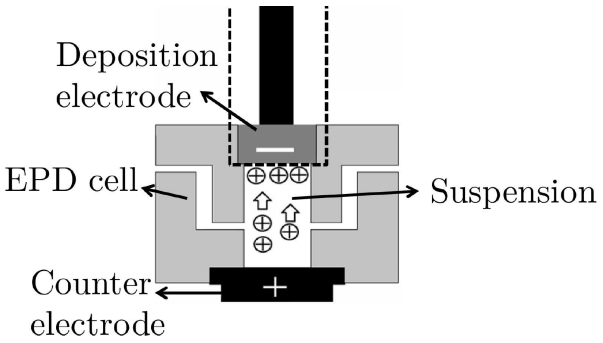

Fig. 2: The electrophoretic deposition (EPD) cell.

2.3. Preheating

For the preheating set-up, a novel building platform was mounted on the (standard) building platform of the DTM Sinterstation 2000. This new building platform was equipped with a vertical tube furnace that contained a zone which could be homogeneously heated to a *preheating temperature (T)* of 800 ± 50°C. Insulation and water cooling were provided all around this assembly, in order to prevent energy losses from damaging the DTM Sinterstation 2000.

2.4. Processing and Process Parameters

Ceramic parts were fabricated using the modified DTM Sinterstation 2000 machine. After layer deposition and preheating at 800 °C, the powder layers were scanned by a CO_2 laser with a maximum power of 100 W, a wavelength of 10.6 μm and a laser beam diameter ($1/e^2$) of 400 μm. An optimized parameter set was found by producing a 2x2 matrix of 4x4 mm^2 squares and varying *laser power (P)*, *scan speed (v)*, *scan spacing (s)* and *scan strategy*. This optimized parameter set was subsequently used to fabricate a 10x10 mm^2 ceramic. The optimized parameters are summarized in table 2. They were found by initially setting the *scan speed* as low as possible to allow for sufficient time for neck formation. The *preheating temperature* was kept as high as possible in order to prevent cracks due to thermal stresses. The first test was done with a *laser power* of 5 W and a *scan spacing* of 40 μm. Since unwanted balling occurred, the energy density was lowered by lowering the *laser power* and increasing the *scan spacing*. Finally, the optimal values of P (2 W laser power) and s (200 μm scan spacing) were obtained.

Table 2: Optimized laser scanning parameters.

P	**s**	**v**	**T**
2 W	200 μm	5.2 mm/s	800°C

2.5. Solid State Sintering

Since no binder material was used, no time consuming de-binding step was needed. However, the directly SLS/SLM'ed ceramics were solid state sintered (SSS) in a furnace (Nabertherm, Germany) in order to make sure that all powder particles were sintered (if not melted). The SSS was done in air at 1600°C for 2 *hours* at a heating rate of 5°C/min.

2.6. Measurements

The fabricated ceramic parts were assessed through density measurements, stereo microscopy and scanning electron microscopy (SEM). The density was measured by the Archimedes method using a Sartorius balance (Analytical

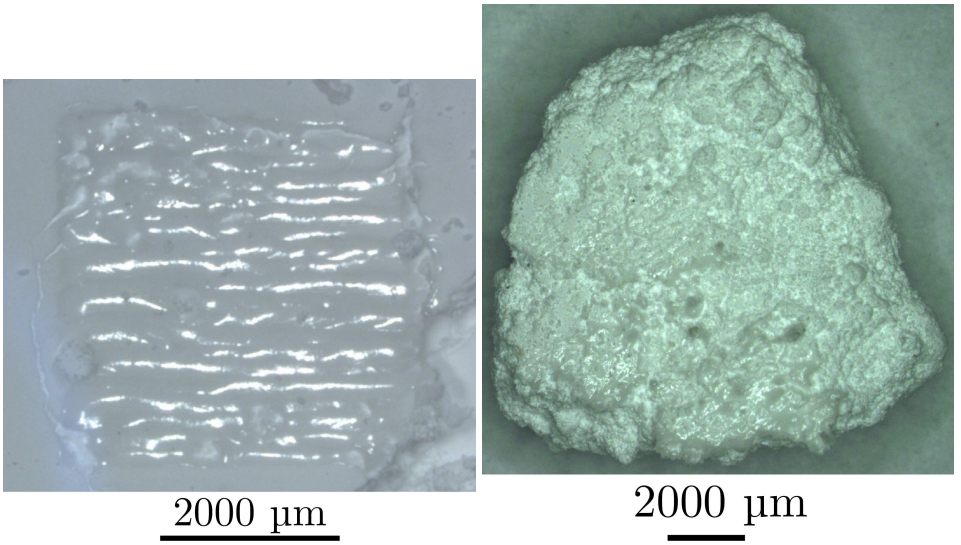

(a) (b)

Fig. 3: The two ceramics that were produced with the optimized parameter set (table 2), ceramic sample 1 (4x4, 5 layers, a) and ceramic sample 2 (10x10, 15 layers, b).

Balances, Sartorius, Germany). A theoretical density of 3.98 g/cm^3 was used for alumina. After density measurements, the ceramics were embedded in epoxy and polished perpendicular to the scan tracks. Digital images could be taken by a stereo microscope (SteREO Discovery V20, Zeiss, Germany). The ceramics were thermally etched in air at 1350°C for 30 min at a heating rate of 20°C/min in a furnace (Nabertherm, Germany) in order to reveal the grain boundaries after polishing. Afterwards, the ceramics were coated with gold-palladium using a sputtering device (Balzers, Switzerland). A scanning electron microscope (SEM XL30 FEG, FEI, the Netherlands) was used for morphology investigations.

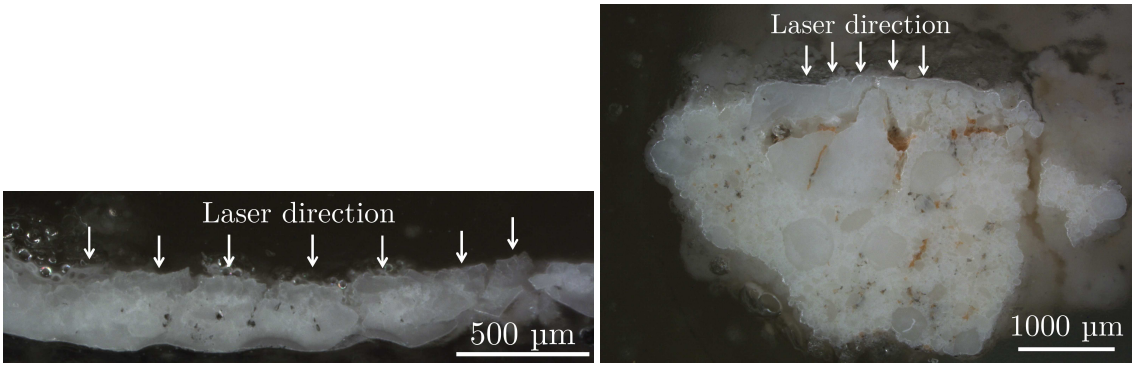

(a) (b)

Fig. 4: Stereo microscopy images of ceramic sample 1 showing upward curling (4x4, 5 layers, a) and ceramic sample 2 showing downward curling (10x10, 15 layers, b).

3. Results

The density of the EPD powder layers deposited with the optimized parameters from table 1 were approximately 57 % (Anné et al. (2006)). This was measured by the Archimedes method using lacquer encapsulation. Subsequent laser scanning was carried out to produce a number of 4x4 mm^2 ceramic parts of 5 layers. One of these ceramics (sample 1, depicted in figure 3a) showed sufficient strength for further research. The parameter set that was used to produce this ceramic was chosen as the optimized laser scanning parameter set (table 2) and another ceramic of 10x10 mm^2 and 15 layers was produced (sample 2, depicted in figure 3b). Ceramic samples 1 and 2 were assessed for density. The relative density of ceramic sample 2 was 85%. Ceramic sample 1, however, was too small and had insufficient mass for a reliable measurement.
Stereo microscopy was performed to visually assess ceramic samples 1 and 2. Ceramic sample 1 (figure 4a) showed upward curling towards the laser beam, whereas ceramic sample 2 (figure 4b) showed downward curling.

Scanning electron microscopy was used to study the quality of the ceramic samples. SEM images of ceramic samples 1 & 2 can be seen on figures 5 & 6 respectively. The unpolished surfaces of the ceramics were investigated. This revealed some interesting features, like the surface cracks on figures 5a & 6b or the solidified alumina droplet on figure 6a. Also, images were taken of a polished cross-section of the ceramic samples and perpendicular to the scan tracks. For ceramic sample 1, the cross-section was taken at the edge of the part, whereas ceramic sample 2 was cross-sectioned in the middle of the part.

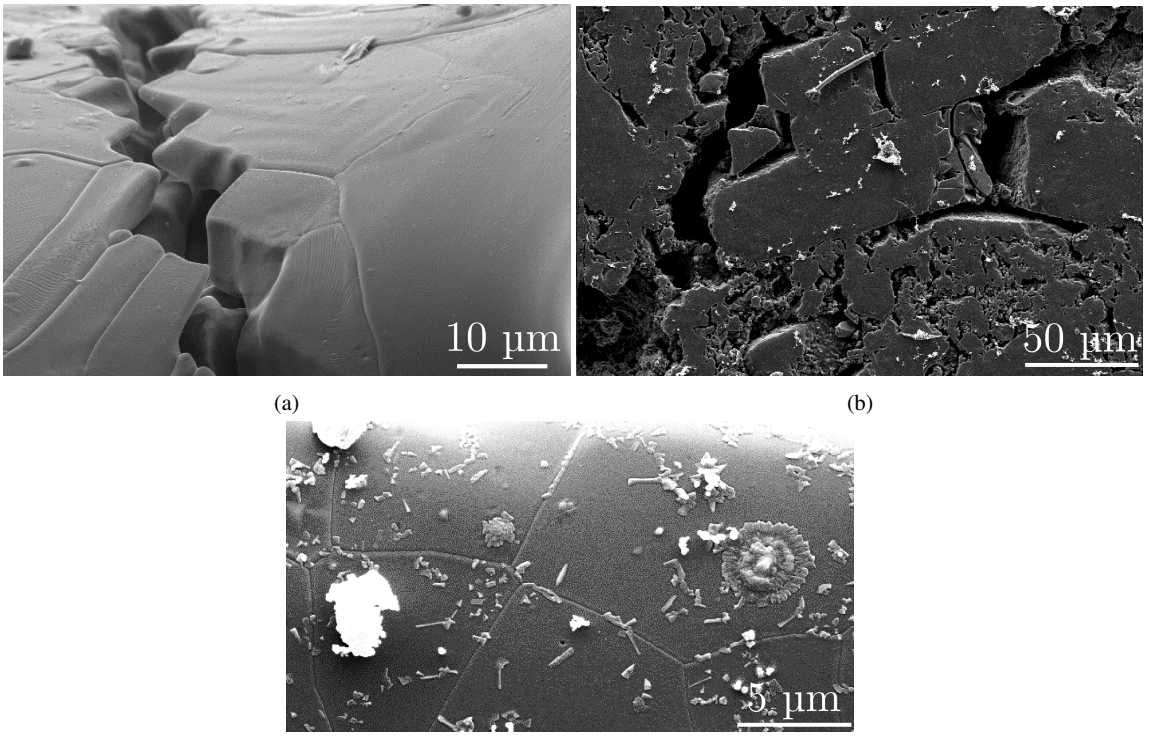

(a) (b)

(c)

Fig. 5: SEM image of an unpolished scan surface with crack (a). SEM images of a polished cross-section, taken at the edge of ceramic sample 1 and perpendicular to the scan tracks (bulk b, top c).

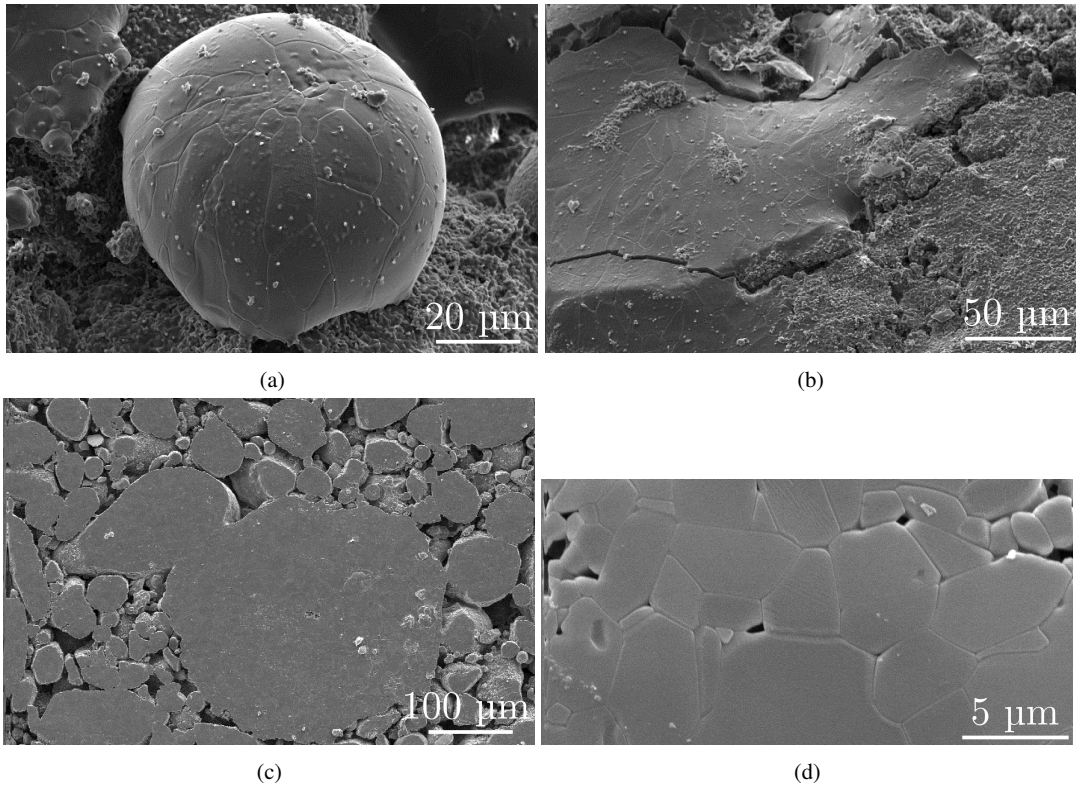

Fig. 6: SEM image of an unpolished scan surface with molten alumina droplet (a) and crack (b). SEM images of a polished cross-section, taken in the middle of ceramic sample 2 and perpendicular to the scan tracks (bulk c, top d).

4. Discussion

The SEM images in figures 5 & 6 should be interpreted carefully. Figure 6a shows a solidified alumina droplet. This proves that a liquid phase was formed during the direct SLS/SLM process. However, not the entire scan track was liquefied: figure 6b shows a solidified liquid phase on the left and a near powder-like structure on the right. It is unlikely that a solidified liquid phase was present in the powder-like zones. The powder-like zones were probably densified during the solid-state sintering (SSS) in the furnace after laser sintering.

Figure 6b reveals a surface crack in ceramic sample 2 which seems to stop where the solidified surface ends. Ceramic sample 1 also contains surface cracks, as depicted on figure 5a. These cracks were probably caused by excessive thermal gradients during direct SLS/SLM causing thermal stresses. This is in agreement with the upward curling of ceramic sample 1 on figure 4a. Possibly ceramic sample 2 showed downward curling because the upward curled pieces broke off during the removal of the ceramic sample from the powder bed.

The bulk microstructure perpendicular to the scan tracks was also investigated. Figure 5b is a cross section at the edge of ceramic sample 1 and figure 6c is a cross section in the middle of ceramic sample 2. These bulk microstructures contain several dense zones which consist of consolidated alumina and are separated by pores. These pores were probably caused by the breaking of the dense EPD layers while sliding from the EPD deposition electrode. During laser sintering, some alumina powder melted, but not enough to fully eliminate all of the pores.

Figures 5c and 6d show the top surfaces of ceramic samples 1 and 2 respectively. The top surface in this case is the surface directly beneath the scan surface. These images can be used to determine grain size. Ceramic sample 1 seemed to have grains larger than 5 μm, whereas ceramic sample 2 had grains close to or smaller than 5 μm. The difference in grain sizes between the two ceramic samples can be linked to the location of the cross section. Since ceramic sample 1

was cross-sectioned near the edge, the grains would have received more laser energy than those of ceramic sample 2, which was cross-sectioned near the middle. Clearly the grain size increases when the laser energy density increases. This proves the assumption that large grains of alumina parts produced through direct SLS originate from large melt pools.

5. Conclusions

A combination of electrophoretic deposition, high powder bed preheating and laser scanning was used to directly SLS/SLM alumina parts. EPD allowed for densely packed powder layers to be produced and deposited into a newly developed building platform that was placed inside a commercial SLS machine. This building platform was equipped with a vertical tube furnace that could homogeneously heat the powder bed up to $800°C$. Because of the densely packed layers and the high preheating temperatures, only a small additional laser energy input was needed to sinter the alumina powder particles. Laser scanning was performed with a *laser power (P)* of $2\ W$, a *scan spacing (s)* of $200\ \mu m$ and a *scan speed (v)* of $5.2\ mm/s$. This resulted in small thermal gradients and melt pools. In this way, large grains caused by large melt pools could be avoided. SEM images revealed that a liquid phase was present during laser processing. However, not the entire scan track was liquefied. This resulted in residual pores in the final parts. Nevertheless, relative densities of 85 % were reached.

Acknowledgements

The work described in this paper was financially supported by the research fund of the KU Leuven under project GOA/2010/12 and by the Research Foundation - Flanders (FWO) under project FWO-G.0956.14N.

References

Subramanian, K., Vail, N., Barlow, J., Marcus, H., 1995. Selective laser sintering of alumina with polymer binders. Rapid Prototyping Journal, volume 1, 24-35.

Liu, Z.H., Nolte, J.J., Packard, J.I., Hilmas, G., Dogan, F., Leu, M.C., 2007. Selective Laser Sintering of high density alumina ceramic parts. Proceedings of the 35th international MATADOR conference, 351-354.

Tang, H.H., Chiu, M.L., Yen, H.C., 2011. Slurry-based selective laser sintering of polymer-coated ceramic powders to fabricate high strength alumina parts. Journal of the European Ceramic Society, volume 31, 1383-1388.

Wilkes, J., Hagedorn, Y.C., Meiners, W., Wissenbach, K., 2013. Additive manufacturing of ZrO_2-Al_2O_3 ceramic components by selective laser melting. Rapid Prototyping Journal, volume 19, 51-57.

Bertrand, P., Bayle, F., Combe, C., Goeuriot, P., Smurov, I., 2007. Ceramic components manufacturing by Selective Laser Sintering. Applied Surface Science, volume 254, 989-992.

Leu, M.C., Pattnaik, S., Hilmas, G.E., 2012. Investigation of Laser Sintering for freeform fabrication of zirconium diboride parts. Journal of Virtual and Physical Prototyping, volume 7, 25-36.

Liu, K., Shi, Y., He, W., Li, C., Wei, Q., Liu, J., 2013. Densification of alumina components via indirect selective laser sintering combined with isostatic pressing. International Journal of Advanced Manufacturing Technology, volume 67, 2511-2519.

Shahzad, K., Deckers, J., Kruth, J.-P., Vleugels, J., 2013. Additive manufacturing of alumina parts by indirect selective laser sintering and post processing. Journal of Materials Processing Technology, volume 213, 1484-1494.

Anné, G., Neirinck, B., Vanmeensel, K., der Biest, O.V., Vleugels, J., 2006. Origin of the potential drop over the deposit during electrophoretic deposition. Journal of the American Ceramic Society, volume 89, 823-828.